Numerical Simulation of Particulate Processes for Control and Estimation by Spectral Methods

Andreas Bück and Günter Klaunick
Thermal Process Engineering, Otto-von-Guericke University, Universitätsplatz 2, 39106 Magdeburg, Germany

Jitendra Kumar
Dept. of Mathematics, Indian Institute of Technology Kharagpur, Kharagpur, West Bengal 721302, India

Mirko Peglow and Evangelos Tsotsas
Thermal Process Engineering, Otto-von-Guericke University, Universitätsplatz 2, 39106 Magdeburg, Germany

DOI 10.1002/aic.12757
Published online September 20, 2011 in Wiley Online Library (wileyonlinelibrary.com).

Results of application of pseudospectral methods, also known as spectral collocation methods, to practical particulate processes including growth, nucleation, aggregation, and breakage are presented. For growth-dominated processes, a considerable reduction in model dimension can be achieved; for pure aggregation and breakage they form a viable option. To handle problems that include aggregation, breakage, and growth phenomena simultaneously, we introduce a hybrid algorithm combining the advantages of spectral methods and cell average or fixed pivot methods for aggregation and breakage. Results are shown for analytical examples as well as real processes taken from the fields of granulation and crystallization. © 2011 American Institute of Chemical Engineers *AIChE J*, 58: 2309–2319, 2012
Keywords: population balance equation, spectral method, granulation, crystallization, model-based control

Introduction

Many products in chemical and process engineering are produced as particulate substances, that is powders. Common processes for the production are, for example, granulation, crystallization, and milling. Particulate products are preferred over other forms, because they are in general more easily transported, stored, and used by customers.

Particles in a powder can be described by a number of distinct properties, for instance the size, moisture content, enthalpy, or the shape. To characterize the products, one can, therefore, introduce the notion of a number density function (NDF) with respect to the interesting particle properties: the NDF then describes how many particles of the powder possess a certain size, moisture and so on.

Industrial requirements on a product can often be stated as preferred (or desired) number density distributions; to achieve these in a specified time in the process, control schemes have to be applied. Another difficulty arises from the fact that the direct measurement of NDFs is very difficult. Consider, for example, the size distribution of particles in a process: in most cases, for example with laser optical probes like Lasentec FBRM (Mettler Toledo, U.S.) or IPP-70 (Parsum GmbH, Germany), a chord length distribution of the NDF is measured. The inverse problem, reconstructing the size distribution from a chord length distribution, is ill-conditioned. To apply modern control schemes or for purposes of process monitoring, model-based measurement schemes (also known as estimators or observers) have to be used to reconstruct the size distribution dynamically from the chord length distribution in a stable, that is, well-conditioned, way.[1]

One common and quite successful approach of modeling particulate processes on a macroscopic scale is the population balance framework (see for instance Hulburt and Katz[2] and Ramkrishna[3]). Here, a balance equation for the temporal evolution of the NDF $n(t, x, \xi)$ under consideration of all particle processes (e.g., growth, aggregation, and breakage) is derived:

$$\frac{\partial n}{\partial t}+\sum_{k=1}^{3}\frac{\partial(G_{x,k}n)}{\partial x_k}+\sum_{k=1}^{K}\frac{\partial(G_{\xi,k}n)}{\partial \xi_k}=\dot{n}_{\text{in}}-\dot{n}_{\text{out}}+p \qquad (1)$$

Here, ξ denotes the vector of internal coordinates (particle properties) and x the vector of external coordinates (spatial position), G_ξ and G_x are the transport velocities along these coordinates, $\dot{n}_{\text{in}}$ and $\dot{n}_{\text{out}}$ quantify in and outgoing particle fluxes, and p is the net rate of production of particles in the system, including particle–particle processes (e.g., aggregation and breakage) and particle creation and depletion due to interactions with a continuous phase (e.g., precipitation and dissolution in crystallization).

The solution of this (in general) multivariable partial integro- differential equation then allows the prediction, monitoring, and control of particulate processes.

Most modern control methods, for example, model-predictive schemes,[4] input-state and input-output linearization,[5] require a finite dimensional state space model of the process

Correspondence concerning this article should be addressed to A. Bück at Andreas.Bueck@ovgu.de.

to be controlled for controller design and implementation. For this the population balance equation (which is of infinite dimension from a system-theoretic point of view) has to be discretized. The discretization is often performed with respect to the internal coordinates; however, a discretization with respect to time is also possible, for example, by using Rothe's methods (cf. Martensen).[6]

Current methods applied in control and simulation of this kind of processes are finite volume methods and finite element schemes. A recent overview on these two classes of methods is given in Mesbah et al.[7] In finite volume methods often only a first-order upwind scheme is used for the discretization of growth terms. In Mesbah et al.,[7] it is shown that to preserve a certain accurracy and stability in the solution, a fine grid, that is, a fine discretization, has to be used. This leads to state space models of a very high dimension, which limits the use of these models in control applications due to the complexity of designing the appropriate controllers and realtime constraints. Realtime constraints are a severe limit for the use of optimization-based control algorithms [like nonlinear model-predictive control (NMPC)], as the size of the optimization problem scales with the size of the model (*cf.* Bock and Plitt).[8]

In this work, we will focus on the use of pseudospectral methods, also known as spectral collocation methods, in the field of control and estimation, that is the main goal of our investigations is to evaluate whether spectral methods yield state space models (systems of ordinary differential equations) of a lower dimensions than those resulting by application of the methods mentioned in Mesbah et al.[7] We will present results for particulate processes including growth, nucleation, aggregation, and breakage. In the current literature, some results are given, for example, in the work of Mantzaris et al.,[9] for n-dimensional population balance equations in a biological framework. However, the important processes aggregation and breakage are not covered in general in their work. Another, quite recent, contribution by Dorao and Jakobsen[10] presents an adaptive spectral element method for population balances. However, adaptive grids often complicate the controller or observer design due to the need of remapping the model results to the process measurements (and vice versa).

We will show that in practical application scenarios—to which we limit our investigations—for a given accuracy considerably less grid nodes are needed in growth dominated processes for pseudospectral methods than in the standard methods currently used in control and estimation. Additionally, the methods can be implemented for two-dimensional (2-D) problems easily, enabling the use in multivariate systems. In the application to aggregation and breakage processes, certain limitations show up that are discussed, and strategies to overcome them are presented, for example, the introduction of a hybrid method to handle problems that include aggregation, breakage, and growth phenomena simultaneously.

Results will be shown and discussed for analytical examples and real process models taken from the fields of granulation and crystallisation.

Process Description

Granulation and crystallization processes can be described on a mascroscopic level by the general population balance Eq. 1. More specific, considering only internal coordinates (particle properties)

$$\frac{\partial n}{\partial t}+\sum_{k=1}^{K}\frac{\partial(G_{\xi,k}n)}{\partial \xi_k}=\dot{n}_{\text{in}}-\dot{n}_{\text{out}}+B_{\text{nuc}}+B_{\text{agg}}+B_{\text{break}}-D_{\text{agg}}-D_{\text{break}} \tag{2}$$

where B_{nuc}, B_{agg}, and B_{break} describe the formation (birth) of particles with the properties $(\xi_1,\xi_2,\ldots,\xi_K)$ due to nucleation, aggregation, and breakage, respectively. Similarly, D_{agg} and D_{break} denote the depletion (death) of particles with these properties due to aggregation and breakage.

Considering binary aggregation only, the birth and death rates can be stated as

$$B_{\text{agg}}=\frac{1}{2}\int_0^v \beta(u,v-u)\,n(t,u)\,n(t,v-u)\,du \tag{3}$$

$$D_{\text{agg}}=\int_0^\infty \beta(u,v)\,n(t,u)\,n(t,v)\,du \tag{4}$$

with v representing the particle volume and β being the aggregation kernel.

Similarly, the breakage of particles can be described by

$$B_{\text{break}}=\int_v^\infty b(u,v)S(u)\,n(t,u)\,du \tag{5}$$

$$D_{\text{break}}=S(v)n(t,v) \tag{6}$$

Here, S is a selection function, that determines the rate of breakage and b is a function that describes how the fragments, are distributed over the properties.

For the growth of particles no general expression can be given—it may depend on the size distribution, for example, in layering granulation (cf. Mörl et al.)[11]

$$G=2\,\frac{\dot{M}_{\text{sus}}}{\varrho\,\pi\mu_2},\quad \mu_2=\int_0^\infty \xi^2 n(t,\xi)\,\mathrm{d}\xi \tag{7}$$

with ξ the particle diameter, $\dot{M}_{\text{sus}}$ the mass flow of solid sprayed on the particles and $\pi\mu_2$ the total surface area of all particles—or only depend on quantities of the surrounding continuous phase, as for instance in crystallization (see, for instance, Ma et al.)[12]

$$G=k\left(\frac{c-c_{\text{s}}}{c_{\text{s}}}\right)^g \tag{8}$$

The parameters k and g are process-specific quantities. The growth velocity then depends on the difference in concentration of the solute in the continuous phase to the saturation concentration c_s. A concentration $c > c_{\text{s}}$ leads to particle formation, whereas $c < c_{\text{s}}$ may lead to dissolution of crystals.

Nucleation is often modeled as an input flux to the system, either as part of the inlet particle flux $\dot{n}_{\text{in}}$ or via the boundary conditions.

In most applications, one-dimensional (1-D) balances ($\dim(\xi) = 1$) are sufficient to describe the process. But even

here the tradeoff between accurracy and realtime constraints in computation has to be made. Applications of multidimensional population balances are also known, for example, in crystallization (2-D, Briesen[13]) and fluidised bed drying [three-dimensional (3-D), Peglow et al.].[14] Here, almost always some kind of model-reduction is performed, for example, derivation of moment models or marginal distributions, to reduce the computational load that arises from the use of the aforementioned standard methods in simulation, estimation, and control.

In the next section, we will give an overview on pseudospectral methods and discuss how and why these can be applied to population balance equations.

Overview on Spectral Methods

Spectral methods are closely linked to the theory of eigenfunctions of differential operators and are known in analysis since Euler and Fourier. They were first considered in numerical analysis in the 1970s and found wide-spread application in the solution of the basic equations of fluid dynamics, for example in weather forecasting, seismic exploration, or multidimensional inviscid flow.[15,16]

Although these methods showed superior performance in many applications, they fell out of favor in the following years because of several problems: they were less intuitive than the finite difference, finite volume, and finite element schemes available at this time and required more effort in programming. Additionally, the handling of complex computational geometries and process nonlinearities was difficult.

But since the early 1990s new interest in these methods is shown, as evidenced by the works of Fornberg,[15] Trefethen,[17] Mantzaris et al.,[9] and Dorao and Jakobsen,[10] among others. In the following we will briefly sketch the main ideas behind pseudospectral methods. For an in-depth treatment, see for instance Gottlieb and Orszag[18] or Canuto et al.[19]

A basic assumption in spectral methods is that the approximation can be expanded as a series:

$$n(t,\xi) \approx \sum_{i=0}^{N} a_i(t)\psi_i(\xi) \tag{9}$$

Here $a_i(t)$ are the so called spectral weights of the spectral modes $\psi_i(\xi)$. The functions ψ_i are chosen once for each problem and are defined on the whole region under consideration—possibly after appropriate rescaling of the problem. This is the main difference to finite element and finite volume methods where local approximations on some subregions are used, for example, lower-order polynomials.

The function set should be complete with mutually orthogonal elements: common choices are the Fourier polynomials, for problems on periodic domains or algebraic polynomials, such as Chebyshev polynomials, for problems on non-periodic domains. If eigenfunctions for a given problem are known then these can also be used to create a spectral method.

The approximation error made in the transition from the infinite dimensional problem to the finite dimensional problem is strongly influenced by the choice of the set of spectral modes and the number of modes N used in the approximation.

For the use in practical application, for example, process monitoring by model-based measurement systems or for controller design and implementation, a suitable set has to be determined once, for instance, by process simulations. This empirical approach has to be taken as it is not possible to calculate the spectral modes analytically for a general nonlinear particulate process.

To determine the time-dependent spectral weights $a_i(t)$ a condition is imposed on the residual

$$\int_{\xi_{\min}}^{\xi_{\max}} \varrho(\xi)\left[\frac{\partial n}{\partial t} + \frac{\partial (Gn)}{\partial \xi} - \dot{n}_{\text{in}} + \dot{n}_{\text{out}} - p\right] d\xi = 0 \tag{10}$$

Substituting n in this equation by Eq. 9 yields general equations for the spectral weights $a_i(t)$ given the set of spectral modes and the weight function ϱ. To apply a numerical method the domain of the problem has to be truncated; this is noted here by $\xi_{\min}$ for the left and $\xi_{\max}$ for the right boundary of the domain, respectively.

The choice of the weight function ϱ determines the type of spectral method. Choosing $\varrho = \delta\ (\xi - \xi_i)$ leads to spectral collocation, that is, the spectral weights $a_i(t)$ are calculated such that the pseudospectral approximation satisfies the population balance equation at the collocation points ξ_i ($i = 1,2,\ldots,N$).

The choice of collocation points is not arbitrary but depends on the spectral modes ψ_i. If algebraic polynomials are chosen then the collocation points must be distributed over the interval in a specific way to prevent numerical difficulties, for example, Runge's phenomenon, in the approximation of the solution.

The specific choice $\varrho = \delta\ (\xi - \xi_i)$ allows to calculate the values of the NDF at the grid nodes, that is, $n(\xi_i)$, directly without using Eq. 9. It is then possible to express differentiation as a matrix-vector multiplication

$$\frac{\partial n}{\partial \xi} \approx \frac{\partial \mathbf{n}}{\partial \xi} = D_\xi \mathbf{n} \tag{11}$$

$$\mathbf{n}^T = [n(\xi_1),\ \ldots,\ n(\xi_N)] \tag{12}$$

The information on the ψ_k is incorporated in the entries of the differentiation matrix D_ξ.

The advantage of spectral methods lies in the accurracy of approximation of derivatives. It can be shown that the approximation error decays faster than $O(N^{-m})$ for every m for sufficiently smooth functions (Trefethen).[17] This means that for a predefined accurracy considerably less number of grid nodes is needed, thus reducing the overall number of differential equations to be simulated. The entries of the matrix D_ξ for one specific method, the Chebyshev spectral collocation method, can be found in the appendix.

Following a similar line of thought, spectral quadrature methods can be derived, for instance, Clenshaw–Curtis quadrature[20] that is an optimal order quadrature formula on the Chebyshev grid.[17] The specific information is also incorporated in the weights of the formula, and the integrand is evaluated at the Chebyshev nodes. The quadrature can then be written as the scalar product of the quadrature weights and the integrand data

$$\int_a^b f(\xi)\, d\xi \approx w^T \mathbf{f} \tag{13}$$

Further details in the derivation of the differentiation matrices (as a limiting case of finite difference methods) and the

integration weigths can be found in the aforementioned book by Trefethen.[17]

In contrast to finite element and finite volume methods the matrix D_ξ is not banded but dense—this is a result of the global approximation approach. In the limit, spectral methods create infinite order approximations—the corresponding differentiation matrices then have infinite bandwith. The denseness of the matrix does not allow the use of highly optimized banded linear solvers, but this is not a serious issue because the dense matrices are of much smaller dimension and the use of dense matrix solvers is not too time consuming.

Inserting these approximations (Eqs. 11 and 13) into the population balance equation 2 then leads to a set of ordinary differential equations for the spectral weights (respectively, the values of the distribution at the collocation points) that can be solved by standard algorithms for differential equations.

Although the aforementioned problems in spectral methods still exist they play only a limited role in particulate processes, because (a) the property space has a simple geometry (line, rectangle, etc.); (b) in application, often sufficiently smooth density profiles are available (often in the shape of Gaussians) that prevent spurious oscillations in the solution due to Gibb's phenomenon; (c) highly optimized standard linear algebra methods can be used (e.g., in the framework provided by Trefethen[17]); (d) extension to multidimensional problems is easy. Additionally, it is expected that the global approximation approach and the high accuracy of spectral integration schemes suit the global particle phenomena aggregation and breakage.

However, as will be shown in the next section for aggregation and breakage processes these expectations are not met. Additionally, further improvement can be made for processes that include growth and aggregation or breakage. Here, a hybrid method—consisting of a spectral method for the growth term and the cell average method (Kumar et al.[21]) for aggregation and breakage—that combines the features of both methods will be presented briefly.

Results

In this section, we present results to illustrate the capabilities and drawbacks of spectral methods in simulation of particulate processes. At first, several nontrivial 1-D population balances, for which analytical solutions are known, are investigated. Following is a real world problem from the area of fluidized bed layering granulation. To show the applicability of the method to multidimensional problems, we will present results for 2-D population balances as well. Here, apart from an analytical example the performance of the methods is investigated for a well-known batch crystallization process.

To judge the results quantitatively, we consider the development of certain moments of the distribution. The ith moment of a 1-D distribution $f : \mathbb{R}_{\geq 0} \times [\xi_{\min}, \xi_{\max}] \rightarrow \mathbb{R}_{\geq 0}$ is defined by

$$\mu_i(t) = \int_{\xi_{\min}}^{\xi_{\max}} x^i f(t,x)\, dx \tag{14}$$

Similarly, in the 2-D case $f : \mathbb{R}_{\geq 0} \times [\xi_{1,\min}, > \xi_{1,\max}] \times [\xi_{2,\min}, \xi_{2,\max}] \rightarrow \mathbb{R}_{\geq 0}$ the (i, j)th moment is defined by

$$\mu_{ij}(t) = \int_{\xi_{1,\min}}^{\xi_{1,\max}} \int_{\xi_{2,\min}}^{\xi_{2,\max}} x^i y^j f(t,x,y)\, dy dx \tag{15}$$

To assess the errors in computation more abstractly, we introduce the (L_1) error measure

$$E(t) = \|n_{\text{analytic}} - n_{\text{numeric}}\|_1 = \sum_{k=1}^{N} |n_{\text{analytic}}(t, \xi_k) - n_{\text{numeric}}(t, \xi_k)| \tag{16}$$

the sum of the absolute pointwise errors evaluated at the grid nodes ξ_k $(k = 1,\ldots,N)$.

In all cases, the aforementioned Chebyshev pseudospectral method is applied, as the computational domain is nonperiodic. Comparisons are made with standard finite volume method (FVM) schemes (with and without flux limiters, e.g., Koren[22]) for growth processes and the cell average method for aggregation and breakage. In the latter cases, the application of the fixed pivot method by Kumar and Ramkrishna[23] is also possible and will yield results similar to the cell average method.

As the domain of the Chebyshev polynomials is the interval $[-1,1]$, the problems have to be rescaled from the physical domain $[\xi_{\min}, \xi_{\max}]$ to this interval. This can be achieved using the following linear transformation:

$$\xi = \Phi(z) = \frac{1}{2}(\xi_{\max} - \xi_{\min})z + \frac{1}{2}(\xi_{\max} + \xi_{\min}), \quad z \in [-1, 1] \tag{17}$$

It has to be noted that this transformation also affects the differentiation and integration operators. Here, the chain and the substitution rule have to be applied once to account for the changes introduced by the scaling.

The resulting model equations are implemented in the MATLAB environment and are integrated with respect to time by the solver ode45, an adaptive Runge–Kutta method (cf. Shampine and Reichelt).[24] For the implementation of the pseudospectral methods, a modified version of the framework provided by Trefethen[17] is used. Analytical solutions used for comparison are calculated by the method of characteristics (MOC, Evans[25]), if not referenced otherwise.

The number of grid nodes for the different methods are chosen such that the moments of the distribution that are conserved by the process, are also conserved by the approximation. Specifically, for a pure growth process this is the conservation of total number (zeroth moment of the number density distribution); for aggregation and breakage, the total volume is conserved (proportional to the first moment if the internal coordinate is the particle volume, and proportional to the third moment if the internal coordinate is the particle diameter). The consistency of higher order moments is also of importance and is used (if appropriate) for comparison of the different methods.

All simulations are perfomed on a standard personal computer (dual core processor with 2.4 GHz and 2 GB RAM). To test whether the potential reduction in state dimension is counterbalanced by an increase in computational time we also present the total wall clock times for the methods.

One-dimensional population balances

Subsequently, the results for several examples of 1-D (one property coordinate) population balances are presented: the

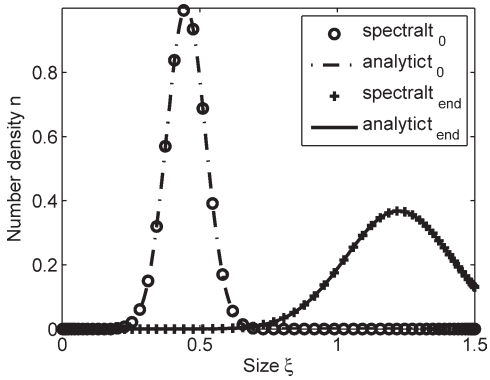

Figure 1. Density distribution *n* for example process 1.

On the left hand side of the figure the initial condition is depicted, on the right hand side the distribution at the end of the simulation is plotted.

analysis starts with a pure growth problem (with size-dependent growth law) and is continued by examples considering breakage and aggregation. As an example from industrial application we present fluidized bed layering granulation.

Example 1. The population balance equation for a simple size-dependent growth problem is given by

$$\frac{\partial n}{\partial t} + \sigma \frac{\partial(\xi n)}{\partial \xi} = 0 \tag{18}$$

For arbitrary initial condition $n(0,\xi) = \varphi(\xi)$ and $\sigma > 0$, the solution is

$$n(t,\xi) = \varphi(\exp(-\sigma t)\xi)\exp(-\sigma t) \tag{19}$$

The resulting distribution starting from a Gaussian initial condition is depicted in Figure 1. Using 64 spectral grid nodes, an error at the end of the simulation time interval $E(t_{\text{end}})$ of 5×10^{-4} is achieved. The wall clock time needed for a simulation interval of $t_{\text{end}} = 2\ s$ is 0.05 s. The first four moments μ_i ($i = 0,1,2$, and 3) of the distribution are consistent with the analytical solution. A finite volume scheme using a flux limiter[22] and the same number of grid nodes needs a wall clock time of 0.5 s with an error $E(t_{\text{end}}) = 0.21$. Increasing the number of grid nodes up to 640 reduces this error to 0.06, but the wall clock time increases to 90 s.

Note that nucleation is not a problem for a spectral method as the boundary of the interval representing the nuclei is always a node in spectral discretisation. However, care has to be taken to generate consistent initial and boundary condition, that is, jumps at $\xi = \xi_{\min}$ have to be avoided, otherwise spurious oscillations will occur in the solution (Gibbs phenomenon). This is possible in many practical applications as nuclei formation also possesses a transient behavior.

Example 2. To test the pseudospectral method we consider aggregation with a constant aggregation kernel $\beta = \beta_0$. For the special initial profile $n(0,\xi) = exp(-\xi)$ the analytical solution for the density is given by Hu et al.[26]

$$n(t,v) = \frac{4}{(\mu_0(0)\beta_0 t + 2)^2} \exp\left(-\frac{2v}{\mu_0(0)\beta_0 t + 2}\right) \tag{20}$$

For the simulation of this process, the birth and death rates of particles are implemented by a spectral Chebyshev quadrature method (Curtis–Clenshaw quadrature).[20] Here, we observe, as in many other numerical methods, that the error in approximation is dominated by the error in evaluation of the birth rate of particles. The reason is the need to evaluate the number density distribution at the volume $v - u$: if it is not an element of the discretized property coordinate, then the value of n is not known and has to be approximated.

The often used approach to approximate the unknown value by the value at the nearest available grid node introduces significant errors in the conservation of total volume, as is seen by the following simple example: consider a Chebyshev grid on [0.001,0.01] with $N = 3$. Then the grid nodes are placed at 0.001, 0.0055, and 0.01. Let $u = 0.001$ and $v = 0.01$, then an approximation of $v - u$ is either 0.0055 (leading to an underestimation of total volume) or 0.01 (leading to an overestimation). This error becomes especially large on coarse nonlinear grids, for instance the Chebyshev grid. Here, the discretization of the interior of an interval is very coarse, leading to large deviations in the distribution and the moments.

Note that this is not the failure of spectral quadrature per se but is caused by the poor approximation of the integrand in its discretized form. Also note that the error may be further increased if a volume-dependent aggregation kernel is used because in $\beta = \beta_0\beta^*(u,v-u)$ the critical term $v - u$ also appears. If, however, $\beta^*(u,v-u)$, is known analytically, then this term can be evaluated exactly.

To summarize, spectral quadrature has no built-in means to guarantee the moment conservation, as do have, for example, the fixed pivot and cell average method, when evaluating the birth and death rates for aggregation of particles. To reduce the errors, the integrand has to be evaluated in a better way.

One approach is to increase the number of spectral collocation nodes. However, due to the special distribution of the nodes—they cluster at the boundaries of the domain—only a very slow rate of convergence is observed. Additionally, the increase in the number of spectral nodes, and thus the number of differential equations, is contradictory to the aim of this investigation, especially due to the clustering effect a very large number might be required.

A second approach locally refines the grid for the evalutation of the rates: on each subinterval $[0,v]$, the distribution $n(t,v^*)$ ($v^* \in [0,v]$) is interpolated using the knowledge on the distribution at the grid nodes in $[0,v]$. The evaluation of the integrand on this local grid then gives a better approximation of the integrals.

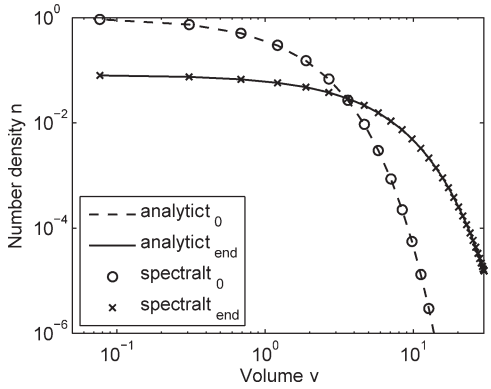

Figure 2. Results for a Chebyshev spectral method for pure aggregation using the interpolation approach (spectral nodes).

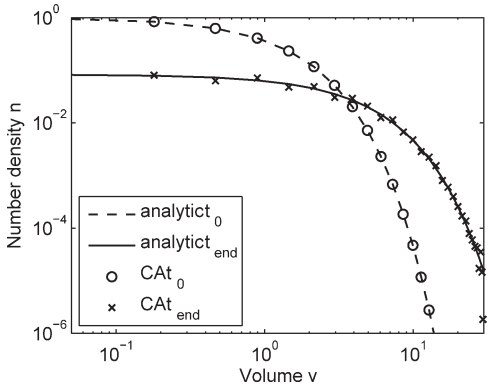

Figure 3. Results of the cell average method for pure aggregation on Chebyshev spectral nodes.

As shown in Figure 2, promising results can be achieved. Here, the total volume is conserved, and the total number of particles is consistent with the analytical solution. A runtime analysis shows that up to 95% of the computation time is spent on the interpolation task. Additionally, the error analysis of this approach is difficult, as the errors of the spectral approach and the interpolation have to be taken into account.

An application of the cell average method on a Chebyshev grid shows that the total volume is conserved and the total number is consistent, but slight deviations in the profile in the interior of the domain, where the grid is coarsest, can be observed (Figure 3).

To summarize the results of this discussion, it can be said that the simple approach of using a spectral quadrature method to evaluate the birth and death rates is not effective due to problems to evaluate the integrands precisely in their discretised forms. The results can be improved by increasing (globally) the number of spectral nodes; however, the accurracy increases only slowly because of the special distribution of the nodes. A (local) refinement in connection with an interpolation improves the result but with an increased effort. Also the error analysis is difficult. Special methods, for example, cell average or fixed pivot method, also work on spectral grids, are easily implemented and yield consistent results in the moments. Regarding the use of spectral methods, no general recommendation can be given: spectral methods are a viable option, but the success of the method depends on the problem.

Example 3. In this example we consider the following population balance equation

$$\frac{\partial n(t,v)}{\partial t} = \int_v^\infty b(u,v)S(u)\,n(t,u)\,du - S(v)n(t,v) \qquad (21)$$

where u,v denote particle volumes, with $b(u,v) = 2/(u - v_{\min})$ and $S(v) = v - v_{\min}$. This equation possesses a breakage-like structure, but is in fact equivalent to a breakage process with a source term due to the occurence of $v_{\min}$ in the denominator of the breakage function b. The reason for this particular choice is that it allows the analytical solution of the population balance equation for a broad class of initial conditions on arbitrary intervals $[v_{\min},\infty)$: given an initial condition of the form

$$n(0,v) = C_1 \exp(-C_2(v - v_{\min})) \qquad (22)$$

with constants C_1 and C_2, the analytical solution can be derived

$$n(t,v) = \left(\frac{C_1}{C_2^2}\right)(t + C_2)^2 \exp(-(t + C_2)(v - v_{\min})) \qquad (23)$$

This solution is derived in an Appendix; in summary, the partial integro-differential equation is first transformed into an equivalent partial differential equation that is then solvable by standard methods.

Note, that for $v_{\min} = 0$, a population balance equation describing pure breakage is obtained. Qualitatively, the solution is an exponential function that becomes steeper and steeper over time (for $C_2 > 0$); in the limit a δ-function at $v = v_{\min}$ is obtained.

A straightforward approach in simulating this process by a Chebyshev spectral integration method yields the following results: the moments μ_0 (total number) and μ_1 (total volume) are predicted consistently for a high number of grid nodes, only. Considering the profile, that is, the number density distribution, one observes deviations from the analytical solution in the interior of the computational domain. This is due to at least two different effects: the grid in the interior is very coarse (see for instance Figure A1 in Appendix), and the fact that to evaluate the integrals the domain is truncated to a maximum volume $[v_{\min},v_{\max}]$. If, for instance, the initial condition is not chosen such that the integrands are sufficiently close to zero as v approaches $v_{\max}$, then a nonnegligible truncation error is made that affects all subsequent computations. To prevent this, $v_{\max}$ has to be chosen sufficiently large, but then also an increase in the number of grid nodes might be required.

These two effects are presented in Figures 4 and 5: in Figure 4, the deviations due to the coarse grid in the interior of the computational domain are clearly visible, leading to an overestimation in the total number and the total volume of particles. To decrease this mismatch in moments, the number of nodes is increased. In Figure 5, 2048 grid nodes are used, but still deviations can be observed.

Example 4. In order to counter these effects the number of grid nodes can be further increased or the described interpolation strategy can be applied: in this example, we consider breakage only. The expressions for the breakage function and the selection function are $b(u,v) = 2/u$ and $S(v) = v^2$. For the initial condition $n(0,v) = exp(-v)$, an analytical solution can be calculated[26]

$$n(t,v) = [1 + 2t(1 + v)]\exp(-(1 + tv)v) \qquad (24)$$

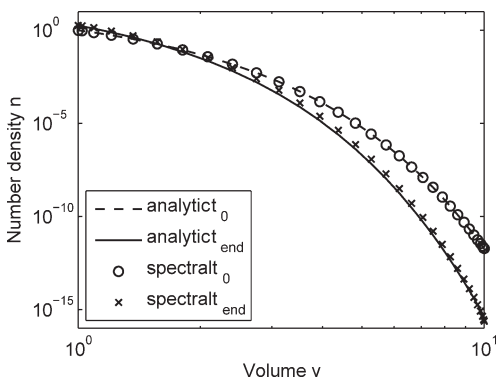

Figure 4. Number density distribution *n* for Example 3 using 32 grid nodes.

The deviations in the interior of the domain lead to an overprediction of total number and total volume of particles.

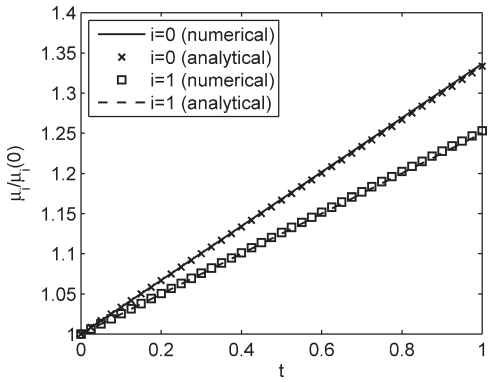

Figure 5. Results for the moments μ_0 and μ_1 using the direct approach to evaluation of the integral terms in the population balance equation of Example 3 (2048 grid nodes).

In Figure 6, it can be seen that the results of the spectral integration using the interpolation approach agree well with the analytical solution. Using 32 spectral nodes a final error $E(t_{\text{end}}) = 9 \times 10^{-3}$ is achieved. Again, most of the time needed for the simulation is spent for the interpolation task, but from the point of controller design or model-based measurement only a small finite dimensional system has to be handled.

Results from Examples 2–4 show that spectral methods are in principle capable of solving the population balances for aggregation and breakage. However, due to the necessary scaling and interpolation of the integrand to evaluate the integrals, the complexity of this approach is high. Additionally, the implementation of the (nonlinear) integral terms is nontrivial. Based on this observation we cannot give a clear statement on the use of spectral methods for aggregation- or breakage-dominated processes. Although in some applications, a model reduction can be achieved, the general estimation of the error is difficult, and the use of widely understood methods, such as cell average or fixed pivot method, seems more appropriate.

In the simultaneous handling of growth and aggregation (respectively, breakage) processes another difficulty arises: for aggregation problems nonlinear grids, often of the type $\xi_i = 2^{i-1}\xi_{\min}$, are preferred as they cover a large interval with few grid nodes. For the calculation of growth terms, the local change at some point is needed, and this is often approximated by a finite difference of the values at neighboring grid nodes. With the above discretisation these gradients become more and more erroneous as the distance to the neighbors gets larger and larger.

To remedy this situation, we now briefly present results for a hybrid algorithm consisting of a spectral method for growth terms and the cell average method for aggregation and breakage terms: the total change in number density due to growth, aggregation, and breakage is decomposed as

$$\frac{d\mathbf{n}}{dt} = \left.\frac{d\mathbf{n}}{dt}\right|_{\text{Growth}} + \left.\frac{d\mathbf{n}}{dt}\right|_{\text{Aggregation}} + \left.\frac{d\mathbf{n}}{dt}\right|_{\text{Breakage}} \tag{25}$$

The change due to growth is evaluated using a spectral method, the change due to aggregation and breakage is calculated by the cell average method.[21] As noted before, by construction, the cell average technique is able to produce consistent results for the moments, total number and total volume, on arbitrary grids, that is, also on spectral grids. Note that any other method that is able to conserve the moments on arbitrary grids, for example, the fixed pivot method, can be used. In that way, the effects can be handled efficiently with a small number of grid nodes as shown by the following example.

Example 5. We consider here another example taken from Hu et al.[26] to illustrate the results of the hybrid method: Taking a growth law $G = \sigma v$ and a constant aggregation kernel $\beta = \beta_0$, an analytical solution for the initial condition $n(0,v) = N_0 \exp(-v/v_0)/v_0$, can be derived

$$n(t,\xi) = \frac{\mu_0(t)^2}{\mu_1(t)} \exp\left(-\frac{\mu_0(t)}{\mu_1(t)} v\right) \tag{26}$$

Using 16 spectral grid nodes a final error $E(t_{\text{end}}) = 1.7 \times 10^{-3}$ is achieved. Wall clock time needed for $t_{\text{end}} = 2$ s is $t_{\text{wall}} = 0.5$ s. The distributions agree very well with the analytical solution as exemplified in Figure 7. The interesting moments total number and total volume of particles are also calculated consistently.

As the cell average method (or the fixed pivot method) are able to produce consistent results for arbitrary

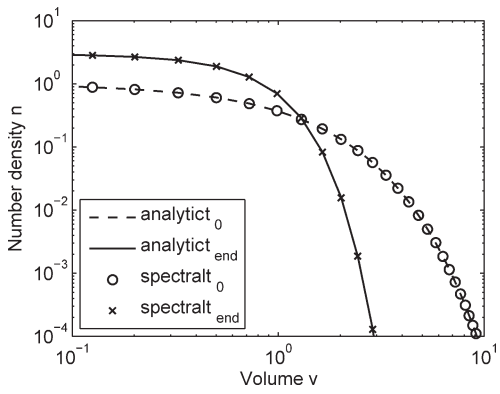

Figure 6. Simulation results for Example 4. The analytical solution (obtained from Hu et al. [26]) and the numerical solution by a Chebyshev spectral method using the interpolation approach with 32 grid nodes are in very good agreement.

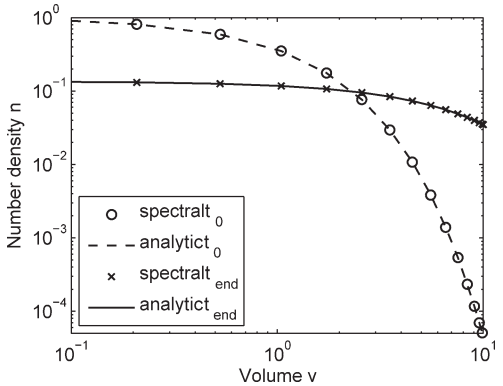

Figure 7. Simulation results for the spectal method—cell-average hybrid method for a population balance equation with simultaneous growth and aggregation.

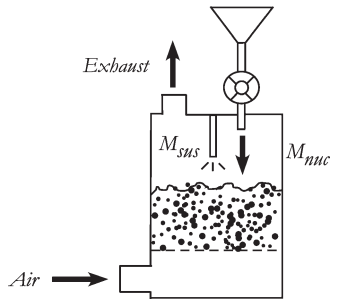

Figure 8. Simple schematic of batch fluidized bed layering granulation process.

aggregation kernels, and the main effect of using the spectral method is to decrease errors in the approximation of the growth terms on nonlinear grids, similar results can be expected for volume-dependent aggregation kernels.

Example – Fluidized Bed Layering Granulation. As a real-world example, we present simulation and experimental results for layering granulation in a fluidized bed. This is a well-known and widely applied industrial process to create free-flowing, dustless powders from liquid suspensions. For a review on the topic, see for instance Mörl et al.[11]

We consider here the batch process depicted in Figure 8, where a suspension is sprayed onto the particles in the fluidized bed. Due to drying—the bed is fluidized by hot air—the liquid in the suspension evaporates, and the remaining solid builds up a new layer on the particles. Considering the particle diameter ξ as the interesting particle property (assuming that the particles are spherical), a growth in particle size can be observed. Manipulating carefully the drying conditions pure growth of the particles, that is, no aggregation or breakage of particles, can be realised (see Ennis et al.).[27]

In the following, we assume a surface-proportional growth law after Mörl et al.[11] that has been widely applied and experimentally verified for this type of process

$$G = 2\,\frac{\dot{M}_{\text{sus}}}{(1-\varepsilon_{\text{shell}})\varrho_{\text{sus}}\,\pi\mu_2}, \quad \mu_2 = \int_0^\infty \xi^2 n(t,\xi)\,d\xi \tag{27}$$

Here, μ_2 is proportional to the total surface area of the particles in the fluidized bed, $\varepsilon_{\text{shell}}$ denotes the porosity of the formed layer.

For the modeling of the particulate phase, the process chamber is virtually divided into two compartments: a spraying zone where suspension is applied onto the particles and a drying zone where only drying of the wetted particles occurs (Ivanova et al.).[28] The reason for this division is the observation that not all particles are at each moment inside the spraying cone created by the nozzle and so not all particles receive solid material for further growth.

Because of the fluidization, a mixing of the particles occurs, that is, a transport from one compartment into the other. The exchange rates are given by the characteristic residence times of the compartments and can be related to the relative sizes of the different zones (Figure 9).

Let n denote the number density distribution of the entire process and n_1 and n_2 the number density distributions in the spraying and the drying zone, respectively, with $n(t,\xi) = n_1(t,\xi) + n_2(t,\xi)$. Then the following system of population balance equations for the different compartments can be derived

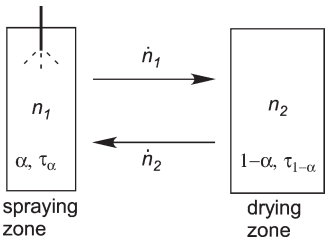

Figure 9. Schematic depiction of the different compartments in the fluidized bed process chamber.

$$\frac{\partial n_1}{\partial t} + G\,\frac{\partial n_1}{\partial \xi} = -\frac{1}{\tau_1}\,n_1 + \frac{1}{\tau_2}\,n_2 \tag{28}$$

$$\frac{\partial n_2}{\partial t} = \frac{1}{\tau_1}\,n_1 - \frac{1}{\tau_2}\,n_2 \tag{29}$$

The parameters τ_1 and τ_2, the characteristic residence times in the spraying and drying zone, obey the following relation to fulfill mass conservation

$$\frac{\tau_2}{\tau_1} = \frac{1-\alpha}{\alpha} \tag{30}$$

where the parameter α represents size of the spraying zone relative to the total size, that is, the size of the spraying zone and the drying zone.

As an real-world example we consider layering granulation of sodium benzoate on γ-alumina carrier particles. The parameters used in the simulation and experiment can be found in Table 1, where the estimate of the shell porosity is obtained by microtomography analysis of the final particles in the experiment.

The results obtained from simulation with 64 spectral nodes ($t_{\text{wall}} = 2.6$ s) and 100 equidistant nodes in a finite volume scheme with flux limiter ($t_{\text{wall}} = 16.1$ s) are compared to measurement results taken from the process ($t_{\text{end}} = 5290$ s). As can be seen in Figure 10, the numerical results of both methods match each other closely and are in good agreement with the measurement. Deviations in the variance of the distributions are due to uncertainties in the model, the parameters τ_1 and τ_2, and the approximation of the initial condition. Note that the spectral method needs approximately one order of magnitude less computation time and only approximately two-thirds of the number of grid nodes of the finite volume scheme, which makes the use of spectral methods in these processes interesting for control and estimation purposes.

Two-dimensional population balances

Example 6. In this example, we consider simple growth in two property coordinates to show the potential of a spectral

Table 1. Process Parameters used in Simulation and Experiment

Initial bed mass m_{bed} (kg)	4.0
Mass flow rate suspension (solid) $\dot{M}_{\text{sus}}$(kg h^{-1})	6.0
Solid density suspension ϱ_{sus} (kg m^{-3})	1440.0
Solid density carrier ϱ_{core} (kg m^{-3})	1280.0
Porosity of created layer $\varepsilon_{\text{shell}}$ (–)	0.74
Relative size of spraying zone α (%)	2.0
Mean residence time spraying zone τ_1 (s)	4.0
Process duration [0,t_{end}]: t_{end} (s)	5290.0

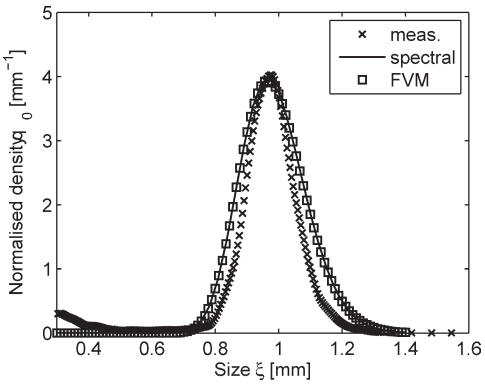

Figure 10. Results from a fluidized bed layering granulation calculated by spectral and finite volume methods compared with experimental results ($q_0(t,\xi) = n(t,\xi) - \mu_0(t)$).

method for this type of problem. We assume the growth rates G_1 and G_2 to be size-dependent: $G_i = k_i cos(\xi_i)$. An analytical solution can also be calculated using an extended method of characteristics. For an arbitrary initial condition $n(0,\xi_1,\xi_2) = \varphi\ (\xi_1,\xi_2)$, the solution to

$$\frac{\partial n}{\partial t} + G_1 \frac{\partial n}{\partial \xi_1} + G_2 \frac{\partial n}{\partial \xi_2} = 0 \tag{31}$$

is given by

$$n(t, \xi_1, \xi_2) = \varphi(s_1, s_2) \tag{32}$$

$$s_i = 2 \arctan\left[\exp(-k_i t) \tan\left(\frac{\xi_i}{2} + \frac{\pi}{4}\right)\right] - \frac{\pi}{2}, \quad i = 1, 2 \tag{33}$$

For a Gaussian initial condition, the results for two points in time are shown in Figure 11. Here, a discretisation with 32 nodes in each direction is used. In the final distribution a maximum pointwise error of $E(t_{end}) = 0.02$ is obtained with $t_{wall} = 0.7$ seconds ($t_{end} = 5$ s). A finite volume method with flux limiter on a 32 × 32 (equidistant) grid yields $E(t_{end}) = 9.42$ and $t_{wall} = 2.6$ s. The error can be decreased by increasing the number of grid nodes but not without increasing the wall clock time, also: on a 100 × 100 grid, the error is decreased to $E(t_{end}) = 5.4$ with $t_{wall} = 28$ s.

Example – Crystallization of KH_2PO_4. As an indicator for the applicability of 2-D spectral methods to real-world prob-

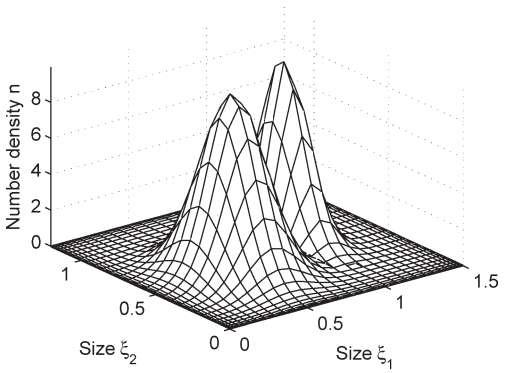

Figure 11. Calculated distributions for Example 6 for two different times on a 32 × 32 grid.

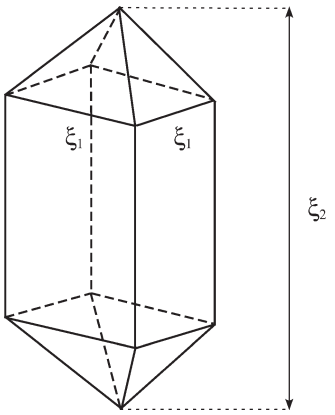

Figure 12. Example of a crystal produced by the crystallisation of KH_2PO_4.

To allow for all configurations between needle-like ($\xi_1 \ll \xi_2$) and pad-like crystals ($\xi_1 \gg \xi_2$), two size coordinates are required.

lems, we consider the batch crystallisation of potassium dihydrogen phosphate (KH_2PO_4). Here, certain crystal configurations are preferred over others, so two size coordinates are needed to describe the produced crystals (Figure 12). This process has been investigated by several groups and mathematical models describing the growth of the crystal size distribution density are available. In the following we use the model equations and parameters from Ma et al.[12] and Briesen.[13]

Using a 64 × 64 nodes Chebyshev grid, a wall clock time of $t_{wall} = 3.4$ s is needed for $t_{end} = 5000$ s. The grid size is chosen such that the shape of the initial distribution is preserved as well as the zeroth total moment μ_{00}. The results for the calculated distributions are shown in Figure 13. Comparative calculations with a finite volume method with a much finer discretisation (512 × 256 nodes) still suffer from numerical diffusion, that is, the shape of the distribution is not preserved. Also, the time necessary for the simulation is approximately one order of magnitude larger: $t_{wall} = 44.1$ s.

Summary and Outlook

In this work, we investigated the use of (pseudo) spectral methods for numerical simulation of particulate systems in view of application in model-based control and estimation schemes. Here, the greatest interest lies in a small model order with a sufficient accurracy in the calculated number density distribution, as the model order greatly complicates the design and implementation of feedback control systems for the property distribution.

By considering prototypical examples of particulate processes—growth, aggregation, and breakage—we were able to show that in case of pure growth processes, a significant reduction in model order—compared to other standard methods (e.g., finite volume methods)—can be achieved under conditions often encountered in practical processes. This was also tested for growth-dominated processes with two property coordinates with similar results. Spectral methods can also be used for the simulation of aggregation and breakage problems; however, here special actions have to be taken to guarantee the consistency of moments. This yields also good results in the approximation of the number density, but the complexity of the method is increased and an error analysis is difficult. For pure aggregation or breakage problems the

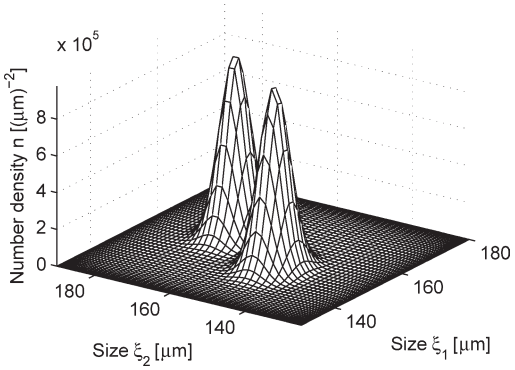

Figure 13. Crystal size distribution for KH_2PO_4 precipitation in water.

Plotted are the distributions for two different points in time.

advantage of spectral methods over specifically tailored methods like cell average or fixed pivot is limited. However, for the important case of simultaneous processes incorporating growth and aggregation, the use of a spectral method for the approximation of the growth term (which has a large influence on the total error on nonlinear grids) can be advantageous as was shown by an example. To verify this encouraging result, a thorough error analysis has to be made. Also, in a further step, this approach will be considered for multivariate processes involving growth and aggregation or breakage.

Acknowledgments

The authors gratefully acknowledge the funding of this work by the German Federal Ministry of Science and Education [Bundesministerium für Bildung und Forschung (BMBF) [as part of the InnoProfile project NaWiTec.

Literature Cited

1. Bück A, Peglow M, Tsotsas E, Mangold M, Kienle A. Model-based measurement of particle size distributions in layering granulation processes. *AIChE J*. 2011;57:929–941.
2. Hulburt HM, Katz S. Some problems in particle technology: A statistical mechanical formulation. *Chem Eng Sci*. 1964;19:555–574.
3. Ramkrishna D. *Population Balances: Theory and Application to Particulate Systems in Engineering*. New York: Academic Press. 2000.
4. Camacho EF, Bordons C. *Model Predictive Control*. London: Springer. 1999.
5. Nijmeijer H, van der Schaft AJ. *Nonlinear Dynamical Control Systems*. New York: Springer. 1991.
6. Martensen E. *Equadiff 6: Proceedings of the International Conference on Differential Equations and their Applications, Lecture Notes in Mathematics*, *The Rothe method for nonlinear hyperbolic problems*. Vol. 1192, Berlin: Springer-Verlag, 1986;387–392.
7. Mesbah A, Kramer HJM, Huesman AEM, Van den Hof PMJ. A control oriented study on the numerical solution of population balance equations for crystallization processes. *Chem Eng Sci*. 2009;64: 4262–4277.
8. Bock HG, Plitt KJ. *A multiple shooting algorithm for direct solution of optimal control problems*. In: *Proceedings of the 9th IFAC World Congress, Budapest*. Oxford: Pergamon. 1984; pp. 242–247.
9. Mantzaris NV, Daoutidis P, Srienc F. Numerical solution of multivariable cell population balance models. II. Spectral methods. *Comput Chem Eng*. 2001;25:1441–1462.
10. Dorao CA, Jakobsen HA. hp-Adaptive least squares spectral element method for population balance equations. *Applied Numer Math*. 2008;58:563–576.
11. Mörl L, Heinrich S, Peglow M. *Fluidized bed spray granulation. Granulation, volume 11 of Handbook of Powder Technology*, Amsterdam: Elsevier B. V., 2007:21–188.
12. Ma DL, Tafti DK, Braatz RD. High-Resolution Simulation of Multidimensional Crystal Growth. *Ind Eng Chem Res*. 2002;41: 6217–6223.
13. Briesen H. Simulation of crystal size and shape by means of a reduced two-dimensional population balance model. *Chem Eng Sci*. 2006;61:104–112.
14. Peglow M, Cunäus U, Kettner C, Metzger T, Tsotsas E. A population balance approach to continuous fluidized bed dryers. In: Briesen H, Ducoste J, Nopens I, Rieger L, Rios N, Vanrolleghem P, editors. *Proceedings of the International Conference on Population Balance Modelling (PBM2007), 19 – 21 September, Montreal, Canada*. 2007;1–5.
15. Fornberg B. *A Practical Guide to Pseudospectral Methods*. Monograph. Cambridge: Cambridge University Press. 1996.
16. Peyret R, Taylor TD. *Comput Methods Fluid Flow*. New York: Springer. 1983.
17. Trefethen LN. *Spectral Methods in MATLAB*. Philadelphia: SIAM. 2000.
18. Gottlieb D, Orszag S. *Numerical Analysis of Spectral Methods*. Philadelphia: SIAM. 1977.
19. Canuto C, Hussaini MY, Quarteroni A, Zang TA. *Spectral Methods in Fluid Dynamics*. Berlin: Springer-Verlag. 1988.
20. Clenshaw CW, Curtis AR. A method for numerical integration on an automatic computer. *Numer Math*. 1960;2:197–205.
21. Kumar J, Peglow M, Warnecke G, Heinrich S, Mörl L. Improved accuracy and convergence of discretized population balance for aggregation: The cell average technique. *Chem Eng Sci*. 2006;61:3327–3342.
22. Vreugdenhil CB, Koren B. editors. *A robust upwind discretization method for advection, diffusion and source terms*. Notes on Numerical Fluid Mechanics, Vol. 45. Braunschweig: Vieweg. 1993:117–138.
23. Kumar S, Ramkrishna D. On the solution of population balance equations by discretization—I. A fixed pivot technique. *Chem Eng Sci*. 1996;51:1311–1332.
24. Shampine LF, Reichelt MW. The MATLAB ODE suite. *SIAM J Sci Comput*. 1997;18:1–22.
25. Evans LC. *Partial Differential Equations*. Providence, RI: American Mathematical Society. 2002.
26. Hu Q, Rohani S, Jutan A. New Numerical Method for Solving the Dynamic Population Balance Equations. *AIChE J*. 2005;51:3000–3006.
27. Ennis BJ, Tardos G, Pfeffer R. A microlevel-based characterization of granulation phenomena. *Powder Technol*. 1991;65:257–272.
28. Ivanova N, Bück A, Peglow M, Tsotsas E. Continuous Pellet Coating for the Pharmaceutical Industry. In: Palzer S, Salman A, Hounslow M, editors. *Proceedings of the 5th International Granulation Workshop*, Lausanne (CH). 2011:1–14.

Notation

Spectral weights, modes	a, w, ψ
Number density distribution	n
Moment of distribution	μ
External (spatial) coordinate	x
Internal (property) coordinate	ξ
Particle volume	v
Particle growth rate	G
Particle fluxes	$\dot{n}_{\text{in}}$, $\dot{n}_{\text{out}}$
Birth rate of particles	B_{agg}, B_{break}
Death rate of particles	D_{agg}, D_{break}
Selection function	S
Breakage function	b
Aggregation kernel	β
Mass flow rate of suspension	$\dot{M}_{\text{sus}}$
Porosity	ε
Solute concentration	c
Solid density	ϱ_{core}, ϱ_{sus}
Residence time	τ
Time	t

Appendix

Chebyshev spectral collocation

For a spectral method using the Chebyshev polynomials as spectral modes ψ_k, the $N + 1$ grid nodes have to be chosen such that $\xi_k = cos(k\pi/N)$, $(k = 0,\ldots,N)$. Note that the ξ_k range

in the interval [−1,1], so that the problem has to be rescaled. The distribution of nodes along the axis is not uniform as can be seen in Figure A1. In fact, the nodes are uniformly placed on the unit circle and then projected onto the axis yielding a very fine disretisation at the boundaries of the interval.

The entries of the differentiation matrix D are then given by (cf. Trefethen[17])

$$D_{00} = \frac{2N^2+1}{6} \qquad D_{NN} = -\frac{2N^2+1}{2} \tag{34}$$

$$D_{jj} = -\frac{\xi_j}{2(1-\xi_j^2)} \quad j = 1,\ldots,N \tag{35}$$

$$D_{ij} = \frac{c_i}{c_j}\frac{(-1)^{i+j}}{\xi_i - \xi_j} \quad i \neq j,\ i,j = 0,\ldots,N \tag{36}$$

where

$$c_k = \begin{cases} 2, & k = 0, k = N \\ 1, & \text{otherwise} \end{cases} \tag{37}$$

Analytic solution of Example 3

We consider a process described by the following population balance equation

$$\frac{\partial n(t,v)}{\partial t} = \int_v^\infty b(u,v)S(u)\,n(t,u)\,du - S(v)n(t,v) \tag{38}$$

where u,v denote particle volumes, with $b(u,v) = 2/(u - v_{\min})$ and $S(v) = v - v_{\min}$. As was mentioned already in the main text, this balance equation has the structure of a breakage process but due to the modifications in the selection function and breakage rate, this is, the occurrence of $v_{\min}$, this is a breakage process with an additional source.

We focus on the solution of the population balance equation on the interval $[v_{\min},\infty)$ for arbitrary initial conditions of the form:

$$n(0,v) = C_1 \exp(-C_2(v - v_{\min})) \tag{39}$$

where C_1 and C_2 are non-zero constants.

Inserting the rate expressions into the equation yields

$$\frac{\partial n(t,v)}{\partial t} = \int_v^\infty 2\,n(t,u)\,du - (v - v_{\min})n(t,v) \tag{40}$$

A direct solution of this partial integro-differential equation is difficult due to the lack of standard methods, so the problem is transformed into an equivalent partial differential equation (PDE). Differentiating (partially) the equation with respect to v yields

$$\frac{\partial}{\partial v}\left(\frac{\partial n(t,v)}{\partial t}\right) = \frac{\partial}{\partial v}\int_v^\infty 2\,n(t,u)\,du - n(t,v) - (v - v_{\min})\frac{\partial n(t,v)}{\partial v} \tag{41}$$

An application of Leibniz' rule to the parameter-varying integral (v being the parameter) then leads to the equivalent PDE

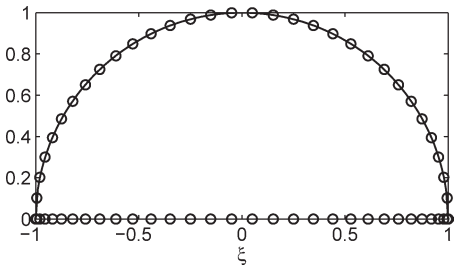

Figure A1. Grid node distribution in the Chebyshev spectral method.

Note that the nodes cluster at the boundaries of the interval yielding a coarser discretisation in the interior of the domain. The nodes are placed on the axis by first distributing them uniformly on the unit (semi) circle and then projecting them orthogonally onto the axis.

$$\frac{\partial}{\partial v}\left(\frac{\partial n(t,v)}{\partial t}\right) = -2\,n(t,v) - n(t,v) - (v - v_{\min})\frac{\partial n(t,v)}{\partial v}$$
$$= -(v - v_{\min})\frac{\partial n(t,v)}{\partial v} - 3n(t,v) \tag{42}$$

Limiting the solution to the specified class of initial conditions and observing the fact that exponential functions remain exponential functions under the linear operators differentiation and integration, the following ansatz for the solution can be made:

$$n(t,v) = A(t)\exp(-B(t)(v - v_{\min})) \tag{43}$$

It immediately follows from the initial condition that $A(0) = C_1$ and $B(0) = C_2$.

Inserting this expression into the PDE yields an ordinary differential equation for the unknown functions $A(t)$ and $B(t)$

$$-\dot{B}A - \dot{A}B + \dot{B}AB(v - v_{\min}) = AB(v - v_{\min}) - 3A \tag{44}$$

Reordering with respect to the powers of $(v - v_{\min})$ yields two differential equations for the functions

$$\dot{B}AB = AB, \quad B(0) = C_2 \tag{45}$$

$$\dot{B}A + \dot{A}B = 3A, \quad A(0) = C_1 \tag{46}$$

with the solutions

$$B(t) = t + C_2 \tag{47}$$

$$A(t) = \left(\frac{C_1}{C_2^2}\right)(t + C_2)^2 \tag{48}$$

that can be obtained by standard integration methods, provided that $AB \neq 0$.

The solution to the PDE can then be stated as

$$n(t,v) = \left(\frac{C_1}{C_2^2}\right)(t + C_2)^2 \exp(-(t + C_2)(v - v_{\min})) \tag{49}$$

By substitution, it can be verified that this is also a solution to the population balance equation.

Manuscript received May 3, 2011, and final revision received July 29, 2011.